

Performance characteristics of methanol and kerosene fuelled meso-scale heat-recirculating combustors

V. Shirsat*, A.K. Gupta

Department of Mechanical Engineering, University of Maryland, College Park, MD 20742, United States

ARTICLE INFO

Article history:

Received 4 May 2011

Received in revised form 7 July 2011

Accepted 9 July 2011

Available online 6 August 2011

Keywords:

Meso-scale propulsion

Hydrogen peroxide

Heat recirculation

Micro-thruster

ABSTRACT

A meso-scale heat recirculating combustor has been developed for the combustion of methanol and kerosene fuels with oxygen enriched superheated steam as an oxidizer. The steam oxygen mixture is a surrogate for the decomposition products of hydrogen peroxide, and as such the combustor development is toward meso-scale bi-propellant propulsion. Both the extinction behavior and thermal performances have been examined under partially-premixed and non-premixed configurations of a unique design incorporating heat recirculation. Stable combustion with thermal efficiencies of ~90% has been demonstrated with both methanol and kerosene. Global flame behavior is investigated through direct image photography of the flame that revealed different flame modes at various equivalence ratios (Φ), including “flameless” combustion of kerosene. Density impulse values calculated based on exhaust temperatures and simulated equilibrium gas properties and assuming 1 atm chamber pressure and expansion to vacuum show that the maximum density impulse of kerosene/steam/oxygen combustion to be within 6% of the adiabatic density impulse of hydrazine/nitrogen tetroxide.

© 2011 Elsevier Ltd. All rights reserved.

1. Introduction

The emergence of MEMS manufacturing technology enables the miniaturization of electromechanical systems at unprecedented scales. With respect to the aerospace technology sector this represents the ability to develop satellite components and entire satellite systems that can be both batch manufactured and inexpensively deployed through reductions in the satellites volume [1]. With this in mind, in an attempt to reduce cost and increase access, mission designers have expressed interest in using distributed micro-spacecraft architectures (constellations and clusters) to meet requirements that are currently satisfied by single, expensive, multi-role satellites [2]. In order for these spacecraft to be effective, the designers will require propulsion systems for launcher injection error, drag compensation, constellation phasing, and proximity maneuvering and rendezvous [2,3]. Owing to their low inertia, these maneuvers will require extremely low thrust (milli-Newton (mN) and micro-Newton (μ N)) and low impulse bit. Contemporary satellites requiring low thrust for vernier control rely on electric propulsion; however, chemical propulsion systems, especially those utilizing high specific gravity propellants, provide an alternative on small satellites already stretched for electrical power. Due to its storability, low safety overhead, and high-density impulse (12% higher than hydrazine despite hydrazine's

25% benefit in specific impulse [4]) hydrogen peroxide has found a niche application in Attitude Control Systems (ACS) for small satellites. This has led to a considerable amount of research in developing monopropellant hydrogen peroxide thrusters of the mN and μ N scale [1,5,6]. However, the higher specific impulse of bi-propellant hydrogen peroxide/hydrocarbon (~153% higher than monopropellant) could lead to potentially significant mass and volume reductions and increased Δv over the lifetime of a satellite.

The enabling technology for developing small chemical thrusters has emerged out of developments in micro and meso-scale combustion systems. It is well known that combustion systems are adversely sensitive to scaling since heat loss to heat generation ratios (surface area to volume) induce flame quenching when the combustor is made sufficiently small. In this regard, different small scale-combustion schemes are characterized by the technique employed to overcome thermal quenching. Wu et al. [7] utilized asymmetric “whirl” whereby recirculating flow act as a source of enthalpy and radical species to stabilize flames in geometries close to the quenching distance. Developed as a precursor to a meso-scale thruster the H_2 /air “whirl” combustor demonstrates relatively high characteristic velocity (C^*) efficiency ratios, which is defined as the ratio of hot flow C^* efficiency to cold flow C^* efficiency, indicating high combustion efficiency. Characteristic velocity represents the exhaust velocity of a converging nozzle with a thrust coefficient of one, and is hence related to the enthalpy of the exhaust gas. Additionally, the lack of heat exchangers for heat transfer between products and reactants makes for small overall geometries; however, the combustor characteristic length

* Corresponding author. Tel.: +1 301 405 5311.

E-mail address: vshirsat@umd.edu (V. Shirsat).

Nomenclature

Δv	velocity change (m/s)	ηC^*	C^* efficiency (unit less)
C^*	characteristic velocity (m/s)	I_{sp}	specific impulse (s)
Φ	equivalence ratio (unit less)	ηI_{sp}	I_{sp} efficiency (unit less)
AR	aspect ratio (unit less)	T_{exp}	experimental temperature ($^{\circ}\text{C}$)
V_y	'y' velocity (m/s)	T_{ad}	adiabatic flame temperature ($^{\circ}\text{C}$)
S_L	laminar flame speed (m/s)	C_p	constant pressure specific heat (kJ/kg K)
Re	Reynolds number (unit less)	ρ	density (kg/m ³)

is larger than the quenching distance at standard conditions. Ahn et al. [8] used Pt catalysts to provide a reaction pathway with decreased activation energy, which increased the amount of heat loss the system could tolerate prior to thermal quenching. The use of catalysts is shown to broaden the extinction regime in the low Reynolds number (low heat load) direction and with low chamber temperatures. Sher et al. [9] computationally explored the limits of Homogenous Charge Compression Ignition (HCCI) as a means to miniaturize micro-internal combustion engines. HCCI involves the homogenous reaction of a charge when it is compressed and is not subject to the limitations of normal flame propagation. In these devices the limitations are imposed by frictional losses, charge leakage through the piston cylinder gap, and timing problems. Several researchers have used structural conduction as a means to preheat the incoming reactants without dilution, thus enabling combustion in “sub-quenching” dimensions [8,10,11]. Sub-quenching is defined as any space where the smallest dimension is less than the quenching distance with the reactants and wall held at ambient conditions. The predominant example is the heat recirculating or “swiss-roll” combustor, which utilizes a spiral counter-current heat exchanger to preheat the incoming reactants; the spiral is situated such that the reactants are always outside the products. The concept is a meso-scale adaptation of the large-scale heat recirculating combustors studied by Jones et al. [12] who used this device to burn fuels of low energy content and extend the lean flammability limits of conventional fuels. This enhancement in flammability limits provide heat recirculating combustors with the flexibility for use in either power generation or thrust production depending on the conditions of operation and geometry. Thus far experimental research regarding the extinction criteria and thermal performance of heat recirculating combustors has been entirely focused on the combustion of premixed reactants, one of which is almost exclusively air. This paper focuses on the extinction limits, thermal performance, and flame dynamics of partially premixed and diffusion flames in heat recirculating combustors. The experimental examination has been performed using oxygen enriched superheated steam as an oxidizer (with a steam to oxygen molar ratio of 2–1) and either kerosene or methanol as fuel. The steam oxygen mixture serves as a surrogate for hydrogen peroxide, with the $\text{H}_2\text{O}/\text{O}_2$ mixture ratio tailored to represent the hydrogen peroxide decomposition products.

2. Experimental facility and procedures

2.1. Combustor

A single turn heat recirculating combustor has been designed to accommodate the combustion of liquid propellants. The number of turns was determined through preliminary experiments with propane and air, which indicated that a larger number of heat exchanger turns lead to higher preheat temperatures, which allows the combustor to burn fuel-lean mixtures. However, increase in the number of turns leads to higher heat losses due to the increase

in exchanger area that is in contact with the fluid and heat exchanger residence times. This leads to lower exhaust temperatures for similar heat inputs [13]. A single turn was found to be the minimum necessary to sustain a flame, and thus yielding the highest exhaust enthalpies.

Since the fuel and oxidizer are introduced non-premixed problems associated with low Reynolds number mixing (mixing by molecular diffusion) and vaporization must be addressed. Since fuel evaporation and mixing times can be large compared to the residence time of gases in the combustor the fuel was introduced through a porous heat recuperator. Similar geometrical arrangements have been used by other researchers, demonstrating successful vaporization of kerosene-like fuels that have relatively poor volatility [14]. Two injection schemes have been investigated. The first injects fuel through an upstream heat recuperator made from compressed double-aught steel wool. In this configuration the recuperator is heated through structural conduction with the combustor body, and through heat exchange with the superheated steam and oxygen mixture. The injector is placed as upstream as is viable due to space constraints related to the feed of ignition wires, plumbing, and diagnostics through the back of the combustor. The second configuration injects fuel through an alumina/zirconia porous ceramic heat recuperator placed directly in the combustion chamber, wherein the recuperator receives heat directly from the flame. The exact location was selected such that the interplay between the aerodynamics of the combustion volume and the injected fuel lead to both rapid mixing and flame stabilization. Aerodynamic flame holding is achieved via a step entrance to the combustion chamber, which provides a vortical flow structure and a local recirculation zone, thus recirculating both heat and active species from the products to the reactants. The fuel is injected into the center of the vortex. Fig. 1 shows both the partially-premixed and diffusion configurations that indicate the steam/oxygen inlets, the combustion zone, and the fuel injection location. Both partially-premixed and non-premixed configurations are identical aside from the fuel injection location. Additionally, flow pathlines through the combustion chamber are shown to illustrate the flow structure in the chamber and the direction of fuel injection for the non-premixed configuration.

The combustor was fabricated from a monolithic block of alumina silicate using conventional machine tools. In its green state it has a thermal conductivity of 1.98 W/mK and is fully machineable with low porosity relative to more thermally insulating materials such as zirconium phosphate, which make it a well-suited candidate for use with liquid fuels. For monolithic swiss-roll combustors the utilization of ceramics is critical for a successful combustor since low thermal conductivity materials minimize heat losses from the combustion zone and support large temperature gradients enabling high rates of heat transfer to the reactants [16].

Typically, in a bi-propellant hydrogen peroxide thruster, hydrogen peroxide is decomposed in a gas generator using an appropriate catalyst into superheated steam and oxygen. This happens upstream of the combustion chamber. The global decomposition reaction proceeds according to the following equation:

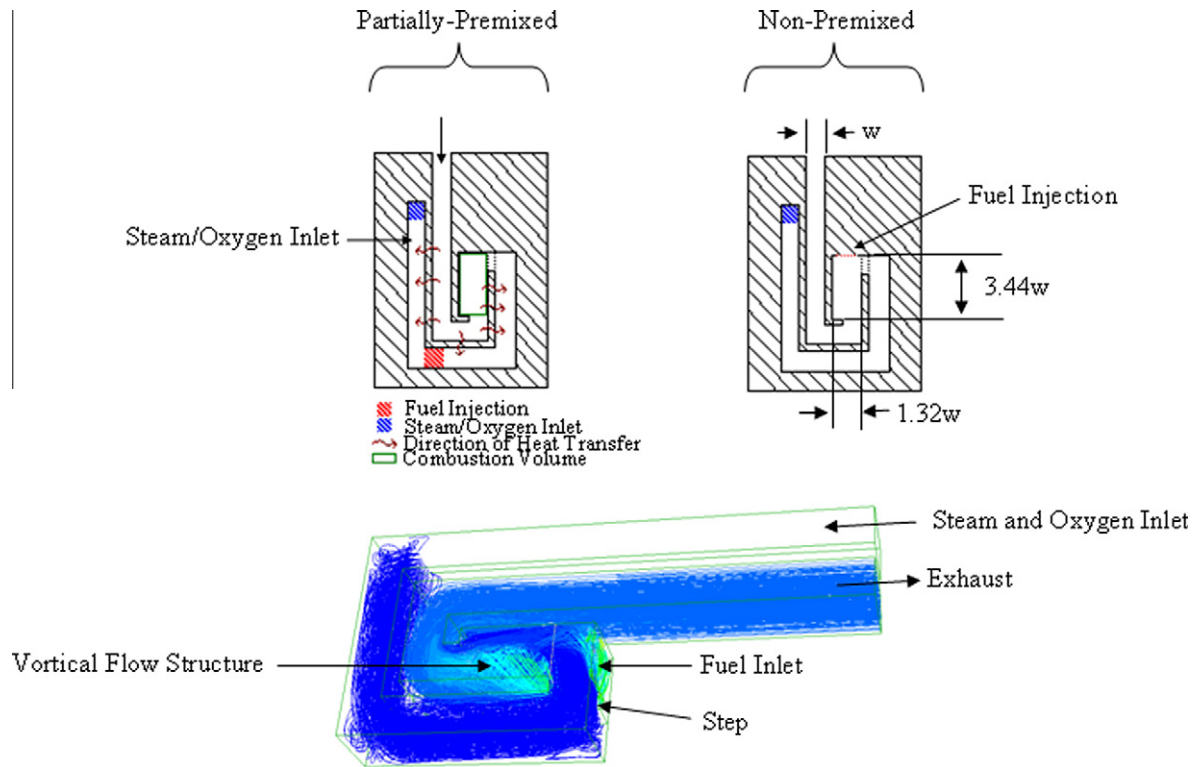
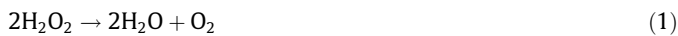


Fig. 1. Combustor schematics highlighting the fuel injection locations.



The decomposition products are passed to the combustion chamber and burnt with fuel. For the experimental combustor the superheated steam/oxygen mixture is generated using a lean burning hydrogen oxygen flame ($\phi = 0.5$) upstream of the combustor, the stoichiometry of which is shown in Eq. (2). This was done in order to study the flame dynamics of the experimental combustor while decoupling it from the complexity of developing a meso-scale hydrogen peroxide gas generator.



For fabrication simplicity the hydrogen oxygen burner and heat recirculating combustor are fabricated into a single unit, with the exhaust from the hydrogen oxygen burner ported into the inlet channel of the heat recirculating combustor. Since the heat release rate from a hydrogen–oxygen flame is larger than the heat release rate from hydrogen peroxide decomposition a thermal isolation cavity is machined in between the steam generator and the heat recirculating combustor. Note that due to the large heat release intimate thermal contact between the hydrogen/oxygen burner and the heat recirculating combustor could unduly influence the results.

Because the product gas temperature of a hydrogen/oxygen flame can easily surpass the adiabatic decomposition temperature of hydrogen peroxide, the experimental conditions that can be realistically tested are limited to those where the steam/oxygen temperature is less than or equal to the hydrogen peroxide adiabatic decomposition temperature. Hence there is an upper limit on the amount of H_2/O_2 that can be burnt before the temperature limit is reached. All the experimental results presented are below this limit.

As mentioned previously, the combustor was fabricated from alumina–silicate. Initial experiments were conducted with the combustor material in its green state. However, stresses possibly

arising from differential thermal expansion of the material and its housing led to cracking at high heat loads, thus limiting the regime over which the combustor could operate. A heat treatment of 45 min at 1050 °C with a ramp rate of 2 °C per minute was used to increase both the hardness and strength of the material with promising results. Additionally, the steam generator was lined with a refractory zirconia blanket to protect the alumina silicate from the hydrogen/oxygen flame, the blanket was both rigidized and surface hardened to prevent deterioration. Fig. 2 shows a photograph of one of the experimental combustors. The top of the combustor is sealed with a quartz window for optical access.

2.2. Experimental facility and procedures

The experimental facility was designed to provide the necessary controls and diagnostics for determining stability regimes and thermal performance of the combustor. Thermal conductivity mass flow controllers were used to control the flow rates of hydrogen and oxygen. The accuracy of each flow controller is $\pm 1.5\%$ of full scale and $\pm 1\%$, respectively. A syringe pump was used to control the methanol and kerosene fuel flow rate. K-Type thermocouples (nickel–chromium versus nickel–aluminum) were used to measure the inlet temperature of the steam–oxygen mixture, the pre-heat temperature, the temperature at the exit of the combustion volume, and the combustor exhaust temperature. A handheld thermocouple data logger recorded the temperatures with an accuracy of 2.2 °C. The thermocouples were unsheathed and the exposed beads yield a blockage ratio of approximately 2.8%; careful installation insured that the thermocouple beads did not make any contact with the combustor material. The ignition source was a 6 V ignition coil driven through a relay triggered by a timing circuit. In the partially premixed configuration at low preheat temperatures the flow velocity is larger than the flame velocity and for the Reynolds numbers, geometry, and mass flow rates in question, repetitive ignition and blow off occurred until the preheat temperature increased the

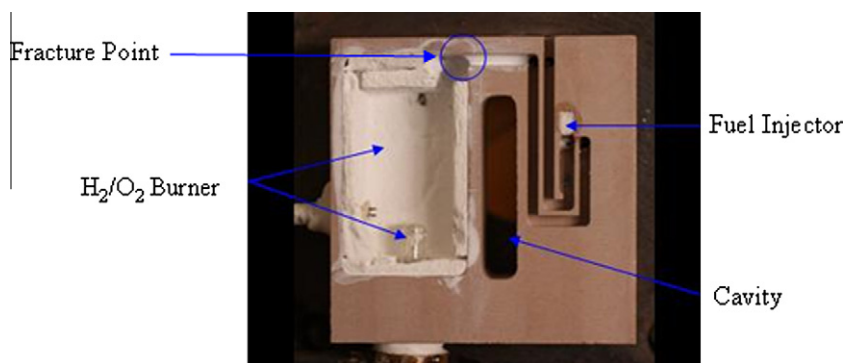


Fig. 2. Photograph of combustor.

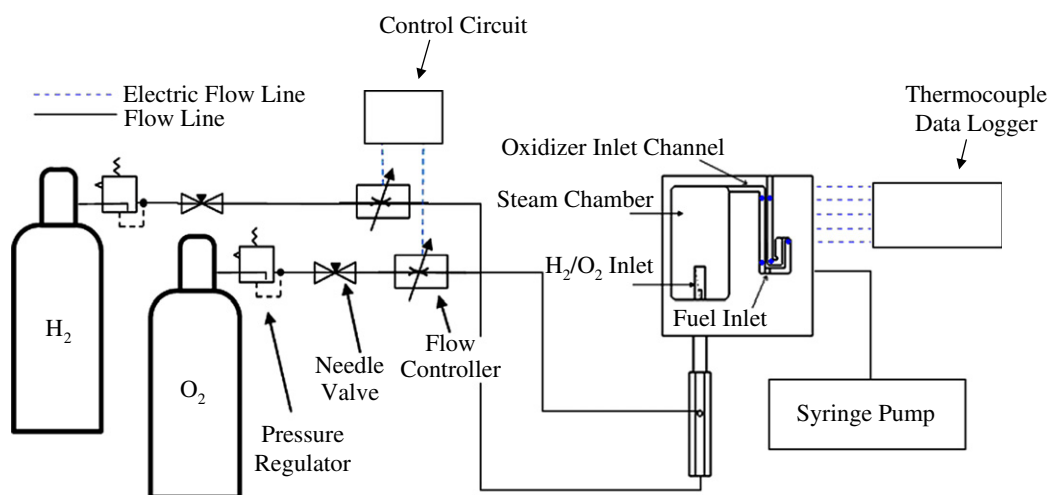


Fig. 3. Schematic of the experimental facility adapted from Vijayan and Gupta [11].

flame velocity to a sufficiently high level. For this reason a high spark frequency is required to stabilize the flame. A schematic diagram of the experimental facility is shown in Fig. 3.

In order to determine the upper performance limit a flame is stabilized at an equivalence ratio close to unity and the hydrogen and oxygen flow rates were incrementally decreased at constant equivalence ratio until a flame was no longer supported. The lower limit was found through an analogous procedure. At each increment the combustor was allowed to reach a steady state, this was determined by thermocouple measurements taken in the exhaust of the combustor. Steady state temperature measurements were taken at each increment to provide a basis for the results and analysis.

3. Results and discussion

3.1. Flame extinction limits and thermal performance

3.1.1. Partially premixed combustion

Fig. 4 shows the extinction regime for the partially-premixed combustor with aspect ratio of 0.5. The extinction regime demonstrates the dual branched behavior that is typical of this type of combustor. The fuel lean limit represents flame blow-off which was observed through the window of the combustor. The rich combustion limit represents a flashback limit where high fuel concentrations and high oxidizer inlet temperatures (between 500 and 550 °C prior to mixing with fuel) combine with low channel velocities allowing the flame to propagate upstream of the combustion

chamber, and stabilize at the fuel injection location. (Note that auto ignition temperature of methanol is 470 °C.) This is analogous to the “out-of-center” reaction zone reported by Ronney et al. [8], however, in the context of this study the flame is considered “extinct” at the flash-back limit.

In Fig. 4, the extinction regime forms the dual branched ‘c’ shape characteristic of heat recirculating combustors. The shape is essentially described by three points, as labeled in the figure: point A is a structural limit (discussed later), point B is the minimum stable Re (rich extinction limit at the minimum heat input), and point C is the rich extinction limit at the maximum heat input. Experimentally, point A is the point where the combustor fractures due to overheating and occurs at roughly the same point for all the tested configurations and is dictated by the material properties. The fracture occurs at the junction of the steam generator and the heat recirculating combustor, indicated by the circle in Fig. 2. Points B and C are associated with flame flashback and are thus sensitive to the combustor geometry, since it plays a role in channel velocities and upstream gas temperature which influences flame velocities.

Since the fuel-lean and fuel-rich extinction limits are blow-off and flash-back limits respectively they are intrinsically related to the velocities and mixture composition at the inlet to the combustion volume. The latter relates to the flame velocity that can be supported by the inlet mixture. Hence extinction limit control should be possible by varying either the inlet geometry (inlet to the combustion chamber, which is analogous to the channel geometry) or the inlet mixture composition. Varying the inlet mixture composition is carried out by changing the concentration of

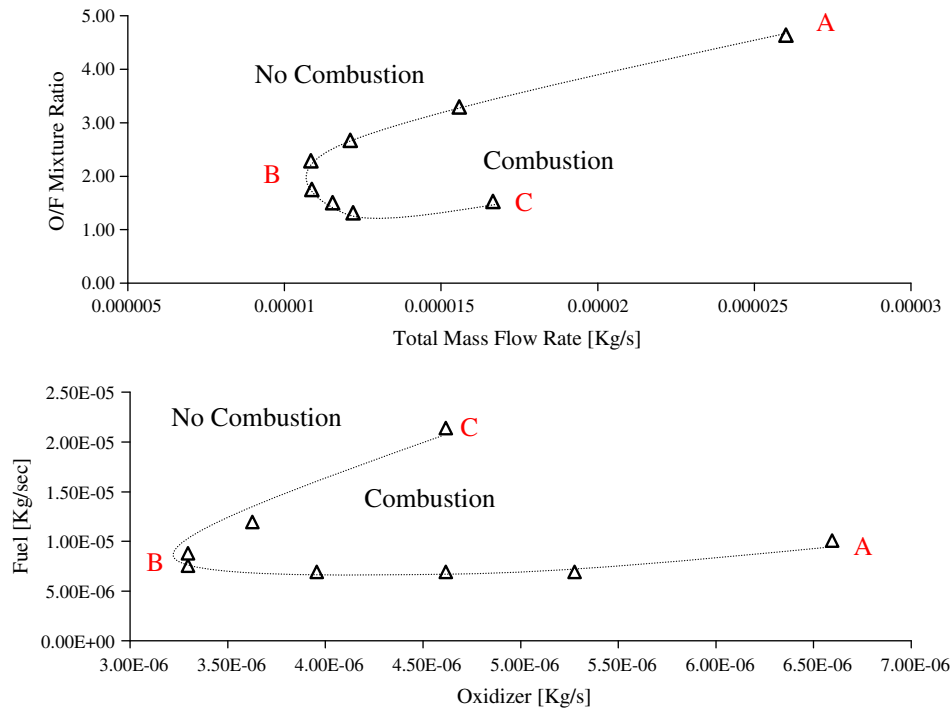


Fig. 4. Extinction regime for the aspect ratio (AR) = 0.5 combustor burning methanol/steam/oxygen.

oxygen in the oxidizer stream, which is analogous to changing the inlet concentration of hydrogen peroxide. One additional combustor was fabricated to examine the affect of channel width on the combustor extinction limits; the channel aspect ratio was sized such that the Reynolds number, based on hydraulic diameter, was constant between the two combustors for identical inlet conditions. Hence the narrower channel is deeper in order to maintain a constant hydraulic diameter. The result is two combustors with channel aspect ratios of 0.5, and 0.4, respectively. Fig. 5 shows the extinction regimes for the two combustors.

Fig. 5 shows that decrease in the channel aspect ratio has little affect on the lean extinction limit and significant affect on the rich extinction limit, and hence the effect of decrease in the aspect ratio is largely to prolong the onset of flame flashback. Flashback occurs when the local velocity is smaller than the flame velocity at a particular location. For the same inlet conditions the smaller aspect ratio channel has a 16.9% higher mean cold flow velocity than the higher aspect ratio channel which would allow for higher channel velocities at low total mass flow rates. However, the cold flow channel velocities are larger than the predicted laminar flame velocities for the entire extinction regime, especially at high global equivalence ratios. (Cold flow velocities ranging from 4 to 10 m/s.) Hence flashback is more likely to occur near the walls where the

velocity field vanishes [17]. Since the combustor operates in a non-premixed mode the flashback propensity for a particular geometry should be related to both the local velocity and the local equivalence ratio in the channel upstream of the combustion volume. Since the Reynolds number in the channel is laminar at best ($100 < Re < 600$) the mixing upstream of the combustion chamber should predominantly be due to molecular diffusion. Isothermal mixing simulations performed using a commercially available CFD software indicate that the mixture immediately upstream of the combustor is only partially premixed, and that large gradients in fuel mass fraction (local equivalence ratio) exist in the channel. Fig. 6 shows the simulation results for methanol at the rich extinction limit of the AR = 0.5 combustor for an inlet methanol flow rate of 0.30 mL/min. From left to right: (i) shows the velocity field at the entrance to the combustion chamber, (ii) shows the equivalence ratio field at the entrance to the combustion chamber and (iii) shows regions on the plane where the local flow velocity in the direction of the channel is smaller than the local flame velocity at the same location ($0 < V_y/S_L < 1$), these are regions where flashback would be more probable.

In Fig. 6(i) the velocity field in the direction of the channel indicates low velocity regions on the bottom left and right hand portions of the channel with higher velocities at the top of the

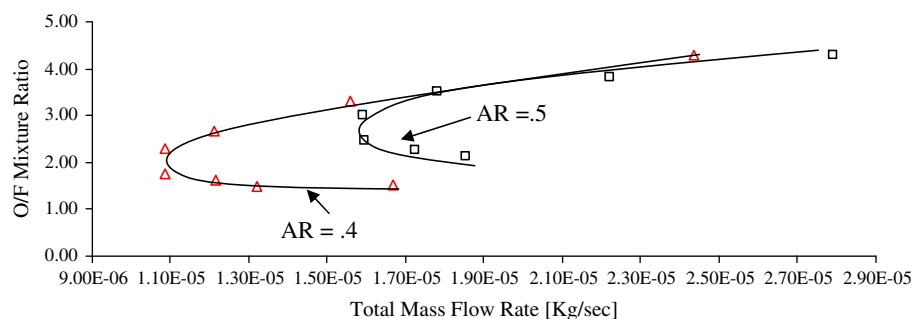


Fig. 5. Extinction limits for the two combustors.

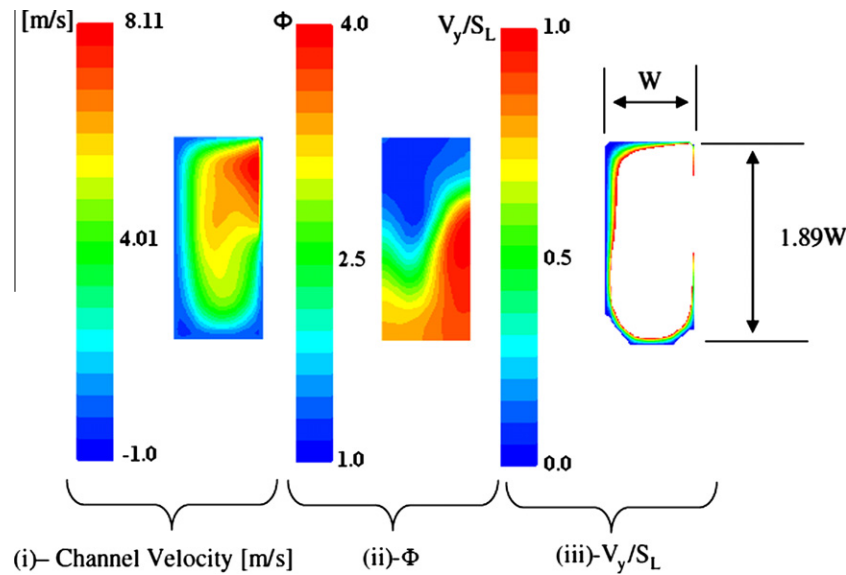


Fig. 6. Channel velocity, equivalence ratio, and flashback propensity on the cutting plane.

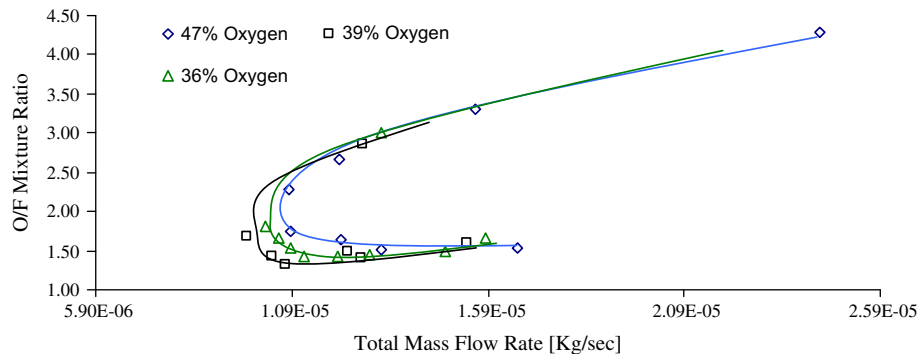


Fig. 7. Extinction regimes at varying oxygen concentrations.

channel close to the entrance to the combustion chamber and a high velocity core flow. In Fig. 6(ii) the reddish¹ region near the bottom of the image represents the developing fuel mass as it diffuses into the oxidizer-rich region above it; due to the high global equivalence ratio stoichiometric conditions are found near the top left hand portion of the channel with fuel rich regions in the high speed core flow. Fig. 6(iii) shows regions where the flashback propensity should be high (regions where $V_y < S_L$), these regions are close to the wall and predominantly at the top left hand corner of the channel, where the local equivalence ratios favor higher flame velocities. The results suggest two conclusions: first, even in the presence of high mean channel velocities the partially premixed combustor can succumb to flame flashback if the local equivalence ratio near the wall can support large flame velocities; and second, the tendency for flashback is a symptom of incomplete mixing. Providing more aggressive mixing upstream of the combustion chamber inlet could alleviate this problem by ensuring that the mixture is closer to the global equivalence ratio, which at the rich extinction limit cannot support high flame velocities.

The sensitivity of the extinction regime to inlet composition was explored by changing the inlet concentration of oxygen in the oxidizer stream; this is analogous to changing the inlet concen-

tration of hydrogen peroxide. The variation in extinction behavior with inlet oxygen concentration is shown in Fig. 7.

Fig. 7 shows that as the inlet oxygen concentration is decreased, the point of minimum stable Re shifts towards lower mass flow rates. It was observed that the decrease in flame velocity was so substantial that the extinction behavior at the rich extinction limit changed from flashback to flame blow-off. This limit is predicted by Ronney [17] in an analytical study and occurs because the reaction zone cools to the point where the time necessary for chemical reaction is larger than the residence time in the chamber, leading to blow-off. However, the cooling is not so substantial that the heat lost from reaction zone is larger than the heat liberated by chemical reaction, which would lead to thermal quenching. Fig. 8 shows temperature based measurements of the enthalpy flow rate into and out of the combustion chamber at a fuel flow rate of 0.3 mL/min. As the mixture is made fuel rich the outflow enthalpy flow rate decreases, and approaches the inflow enthalpy flow rate, where they cross the flame would succumb to thermal quenching; however, the flow velocity is high enough to blow it off prior to this point. It is important to note that combustion of mixtures where the oxygen stream has less than 47% oxygen (100% hydrogen peroxide) was not possible in the non-premixed configuration, discussed later. In the non-premixed configuration the fuel is passed directly from the heat recuperator into the combustion chamber, because of this it receives limited preheat. This is not the case with the partially preheated configuration where the fuel is preheated

¹ For interpretation of color in Figs. 1–8 and 10–22, the reader is referred to the web version of this article.

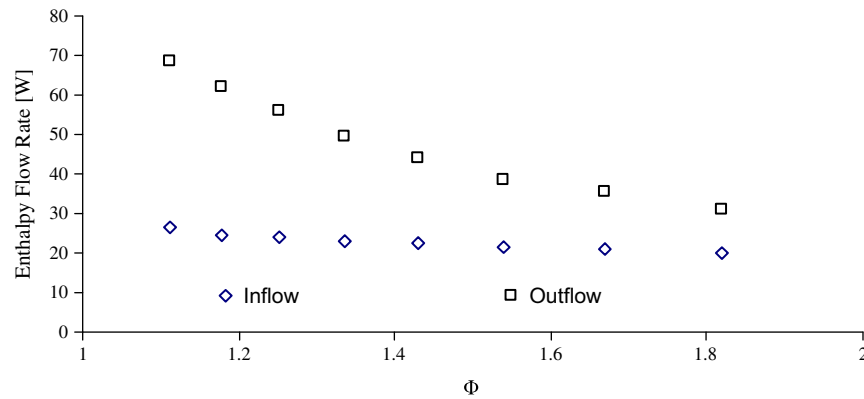


Fig. 8. Enthalpy inflow and outflow to and from the combustion chamber.

along with the oxidizer, allowing for the combustion of weaker mixtures.

The present investigation is centered on the use of the heat recirculating combustor in a propulsion device. The thermal performance is measured based on the specific impulse and characteristic velocity efficiency (ηC^* and ηI_{sp} , respectively) of the combustor. The efficiencies are defined as the ratio of the calculated value based on the measured exhaust temperature and the adiabatic flame temperature for the same conditions. The characteristic velocity and specific impulse are related to the enthalpy of the product gas and is therefore dependent on gas properties, such as specific heat. However, since the gas properties used in the calculation of both C^* and I_{sp} are based on chemical equilibrium of the product gasses they are the same for both the experimental conditions and the adiabatic conditions. Hence the ratio of experimental C^* and I_{sp} and adiabatic C^* and I_{sp} is independent of gas

properties. Eq. (1) shows the relationship used to calculate the efficiencies. Both the efficiencies and the exhaust temperature are shown in Fig. 9, for varying mixture ratio and four different fuel flow rates.

$$\eta C^* = \eta I_{sp} = \sqrt{\frac{T_{exp}}{T_{ad}}} \quad (3)$$

Fig. 9 shows that the maximum efficiencies are found at the fuel lean extinction limit for all four fuel flow rates, and the minimum at stoichiometric conditions with the overall range between ~60% and ~90%. Fig. 9 also shows that the exhaust temperatures increase monotonically as the mixture is made fuel lean. Since the product gasses undergo heat exchange with the reactants and heat loss to the combustor material before exiting the combustor the exhaust temperature is related to both the rate of heat loss from the

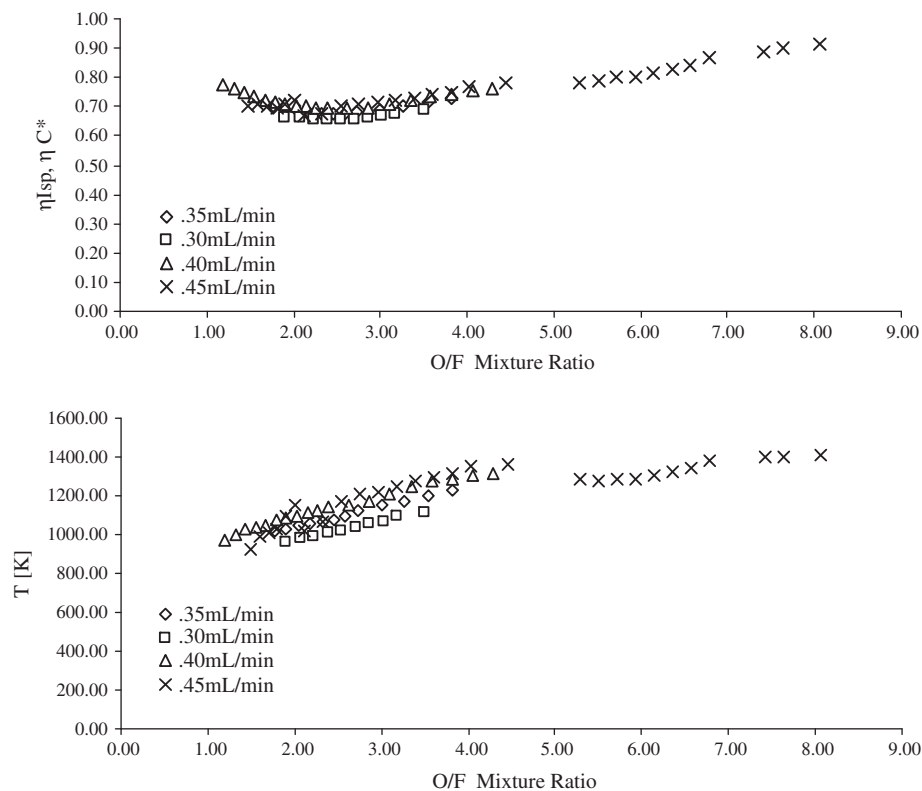


Fig. 9. Thermal performance of the heat recirculating combustor. Top: C^* and I_{sp} efficiencies, bottom: exhaust temperature.

product gas, its temperature as it exits the combustion chamber, and its heat capacity rate (the product of the total mass flow rate and the specific heat capacity). The flame temperature decreases as the mixture is made fuel lean while the heat capacity rate increases. Because of the latter the energy content (enthalpy flow rate in watts) is much larger at lean conditions because of the larger mass flow rate, and the heat exchanger cannot provide a means to lose that energy. This allows the exhaust temperature to increase as the mixture is made fuel lean despite the drop in flame temperature. For this reason, at a particular fuel flow rate, the efficiencies are largest at the fuel lean limits, and at the maximum the exhaust temperature is 83% of the adiabatic flame temperature.

3.1.2. Non-premixed combustion

As mentioned in Section 3.1.1 a second fuel injection configuration was tested whereby the fuel is injected directly into the combustion chamber. This configuration is shown in Fig. 1, and was tested with both methanol and kerosene (grade K1). It is important to note that kerosene combustion was not possible at any condition in the partially premixed configuration. The extinction limits for the methanol flame in non-premixed combustion are shown in Fig. 10, below.

In Fig. 10, Φ represents the global equivalence ratio and no absolute lean extinction limit could be found due to limitations with the experimental facility that was discussed in Section 2.1. Equivalence ratio is defined as the actual fuel air ratio to the fuel air ratio at stoichiometric conditions. The red line labeled Approx. Limit represents the point where the steam/oxygen inlet temperature is larger than the adiabatic decomposition temperature of pure hydrogen peroxide. The green line labeled structural limit is the point where the combustor fractures at the inlet as shown in Fig. 2, and the blue line labeled FREI LIMIT are conditions where

the flame experiences repetitive extinction and ignition events (named Flame with Repetitive Extinction and Ignition (FREI) in the literature [15]). Temperatures were measured at four locations in this configuration, they are: the inlet steam and oxygen temperature, the preheat temperature (which is the inlet to the combustion chamber), the product gas temperature (which is the exit from the combustion chamber), and the exhaust temperature. The four measured temperatures versus equivalence ratio for a methanol flow rate of 0.45 mL/min are shown in Fig. 11.

Fig. 11 shows similar global behavior as was experienced with partially premixed combustion with exhaust temperatures increasing monotonically in the fuel lean direction, with the rate increasing at around $\Phi = 1.5$. It is important to note that the preheat temperatures are always lower than the inlet temperatures unless the combustor is operating in globally rich conditions with $\Phi > 2$. This means that the rate of heat loss from the steam/oxygen mixture is larger than the rate of heat recirculation from the products. Note that in Fig. 11 the trend in product gas temperature, measured at the exit of the combustion volume, is slightly different than the trend in exhaust temperature. Because the temperature is measured at the entrance to the exhaust channel it more closely follows the trend in adiabatic flame temperature, which peaks at slightly rich conditions and drops off in both the rich and lean directions. The exhaust temperature, on the other hand, is subject to heat transfer from the product gas stream to the reactants, and heat loss from the combustor. Because of the large increase in heat capacity rate as the mixture is made fuel lean (at constant fuel flow rate) the exhaust temperature increases monotonously in the lean direction, even through the product gas temperature decreases. Fig. 12 shows the steam oxygen enthalpy flow rates at the inlet and preheat locations versus equivalence ratio during methanol combustion (labeled after) and the enthalpy flow rates at the inlet

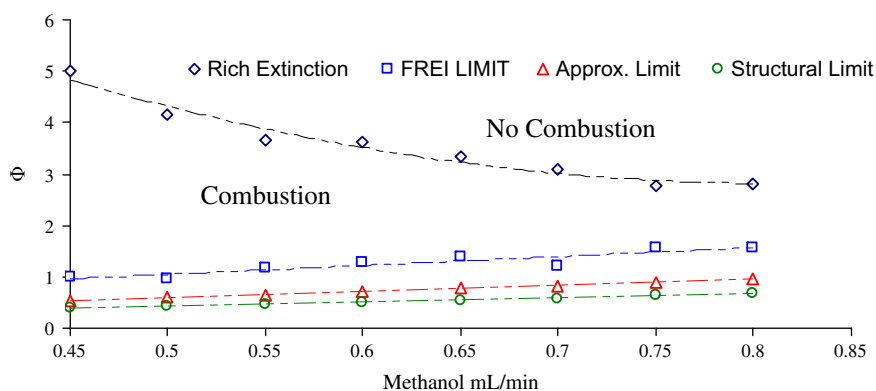


Fig. 10. Extinction limits for non-premixed combustion of methanol.

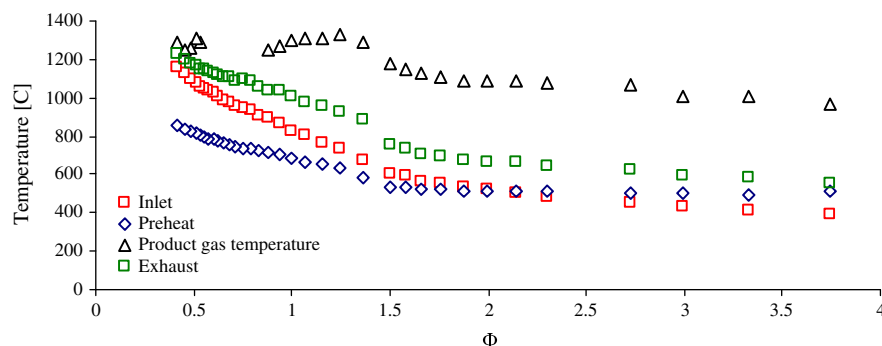


Fig. 11. Inlet, preheat, product gas, and exhaust temperatures for non-premixed methanol combustion.

and preheat conditions without the methanol flame (labeled before).

Fig. 12 shows that the inlet enthalpy flow rates at the before and after conditions are roughly equal. Assuming they are the equal, the before and after preheat conditions indicate that the value of heat recirculation in this configuration is to lessen the amount of heat lost from the inlet oxidizer stream, but not to increase its temperature unless at very rich conditions. This means that insulating the inlet channel with an extremely low thermal conductivity material such as aero-gel, or vacuum seal, could be used to further mitigate the heat loss and possibly increase the oxidizer temperature. As seen in Fig. 10 increase in the preheat temperature would have no impact on extending the lean flammability limit in this configuration since it is already extended as far as possible; however, higher preheat temperatures would result in higher flame temperatures and hence higher efficiencies and larger thermal output. The thermal efficiency of the non-premixed combustor is shown in Fig. 13. As in Fig. 9, the efficiencies are reported in terms of I_{sp} and C^* efficiency as per Eq. (1). The thermal efficiency of the partially premixed combustor for the same fuel flow rate (0.45 mL/min) is also shown for comparison.

Overall, the partially-premixed and non-premixed combustors demonstrate similar trends in thermal efficiency with minimums in the slightly fuel rich regime and maximums close to the fuel lean limit. The maximum efficiency is found at the lean extinction limit with a 1.4% variation in efficiency between the two combustors. The jump in efficiency in the partially premixed case at $\Phi = 1.5$ is an artifact of the experimental facility since the flow controllers were changed at this point to accommodate higher flow rates. Additionally, Fig. 13 shows that the combustor is able to support a flame in the combustion chamber over a much broader range

of equivalence ratio, since in the non-premixed case the flashback mechanism of flame extinction is irrelevant.

As mentioned previously, FREI instability behavior was observed in the lean regime and is present at all conditions between the lines labeled FREI limit and Approx. Limit in Fig. 10. High speed cinematography was used to investigate the FREI instability behavior in non-premixed methanol/steam/oxygen combustor with Kanthal wire igniters. Since the flame surface is not clearly visible the grayscale intensity was tracked at two locations inside the combustion chamber and one location just downstream of the combustion chamber and the intensities used to infer the extinction and re-ignition event. The time trace of the intensities is shown in Fig. 14; the line labeled “Downstream Location” is the intensity at the product gas thermocouple, the line labeled “In Chamber 1” is the intensity at the downstream ignition wire, and the line labeled “In Chamber 2” is the intensity at the upstream ignition wire.

From the time history it can be inferred that after the initial intensity decay due to flame extinction, cyclic re-ignition and extinction events occur in pulses roughly separated by 0.175 s or 5.7 Hz. The peak intensity rises with each subsequent pulse because each prior pulse heats the combustor slightly and the next pulse comes before the heat can be lost. This continues until the flame is re-stabilized inside the combustion chamber. The high speed video shows that the re-ignition occurs in the exhaust and the flame propagates back upstream. A proposed mechanism for re-ignition is shown in Fig. 15.

In Fig. 15, drawing (i) shows a flame stabilized in the combustion chamber with hot steam and oxygen mixture entering through the inlet channel and hot combustion products exiting through the exhaust channel. The direction of heat transfer is from the hot combustion products to the steam oxygen mixture, as can be seen

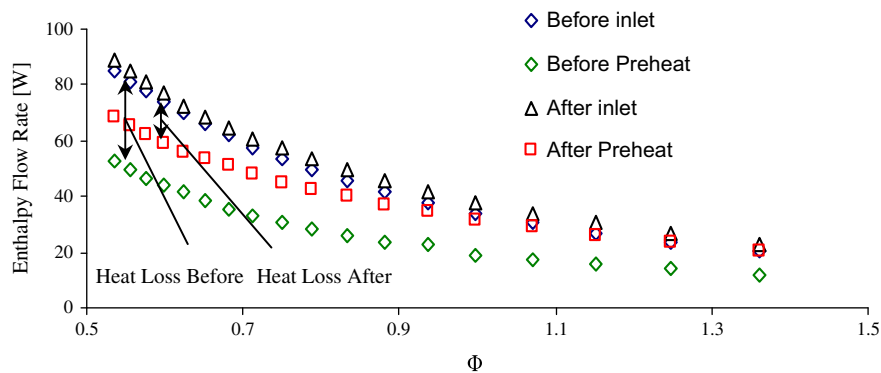


Fig. 12. Inlet and preheat enthalpy flow rates before and after combustion.

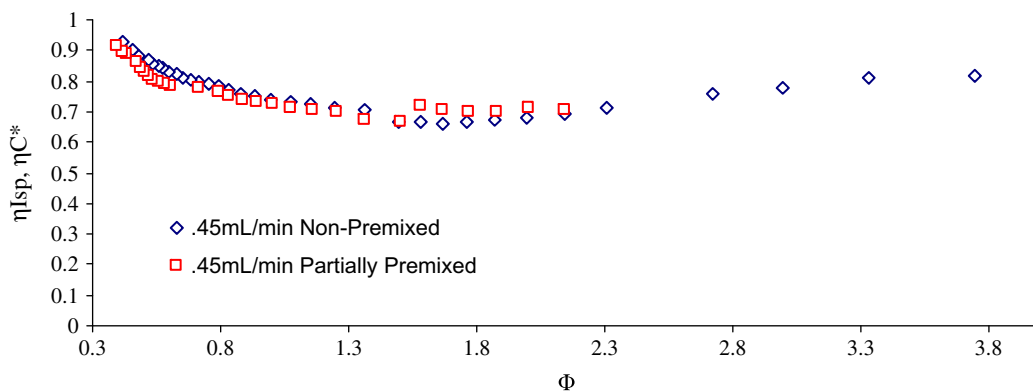


Fig. 13. Thermal efficiencies of partially premixed and non-premixed combustor.

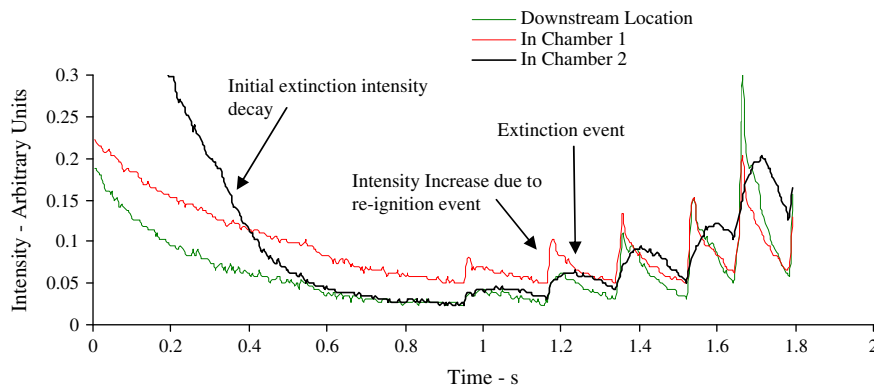


Fig. 14. Time trace showing the extinction and re-ignition process.

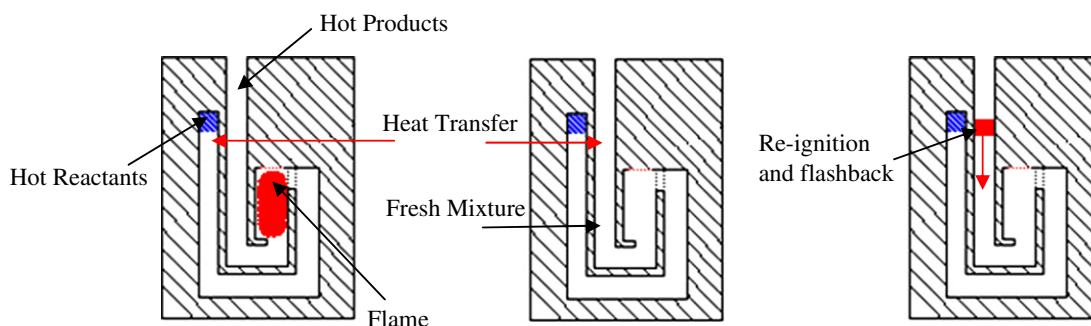


Fig. 15. FREI mechanism for the heat recirculating combustor.

in Fig. 11. In drawing (ii) the flame is extinct, hot steam and oxygen are still entering through the inlet channel; however, fresh mixture at a lower temperature is exiting through the exhaust channel; here the direction of heat transfer is from the steam oxygen mixture to the exhaust. In drawing (iii) the heat input from the steam oxygen mixture causes re-ignition of the reactant stream flowing out of the exhaust; with no-where to anchor, the flame flashes back into the combustion chamber and re-stabilizes. It is important to note that a cause for extinction is not established.

Global flame images of the partially-premixed and non-premixed combustor also show notable differences in flame location and shape. Fig. 16 shows flame images of the partially premixed and non-premixed combustors at roughly the same global equivalence ratio ($\Phi = 1.0$ and $\Phi = 1.15$, respectively), and subsequent images of the non-premixed combustor at equivalence ratios of $\Phi = 0.83$ and $\Phi = 0.68$. Although the flame surface is not explicitly visible in any of the images the high luminosity from the walls in the partially-premixed combustor just left of center in the combustion chamber suggests a localized reaction zone at that location. The wall luminosity in the non-premixed combustor is more uniform and suggests a broader reaction zone. In the non-premixed combustor as the global equivalence ratio is decreased at constant fuel flow rate the flame appears to be pushed further away from the combustor inlet. This is made apparent by the glowing of the downstream ignition wire and product gas thermocouple.

Note that the size of the Kanthal ignition wires (1/64 in. diameter) is significant compared to width of the combustion chamber, and at $\Phi = 0.83$ and $\Phi = 0.68$ it appears that the flame may be stabilized on the downstream ignition wire and the product gas thermocouple. In order to test this, a second variation of the non-premixed combustor was fabricated without the product gas thermocouple and with silicon carbide (SiC) igniters that are flush mounted with the bottom of the combustor, so that nothing is pro-

truding into the combustion chamber. Fig. 17 shows the flame images for the non-premixed combustor with flush mounted SiC igniters.

Based on the wall luminosity the non-premixed combustor with SiC igniters also shows a broad reaction zone as compared to the partially-premixed case, with regions of higher luminosity close to the exit of the chamber. What is notable is that changing the ignition scheme changes the dynamics of the flame in several ways. First, the reaction front does not move away from the fuel injector as the equivalence ratio is decreased. Second, the combustion with the wire igniters is very loud, with high pitched acoustics over the entire extinction regime which is accompanied by motion of the flame inside the combustion chamber as seen from high speed cinematography (at 200 fps). Over the same conditions, the combustor with the flush mounted SiC igniters is silent with no apparent flame motion; this is accompanied by higher exhaust temperatures than the combustor with wire igniters. Finally, the combustor with SiC igniters does not demonstrate any FREI behavior. The exhaust temperatures and thermal efficiencies of the non-premixed wire igniter combustor and non-premixed SiC igniter combustor are shown in Fig. 18, for a methanol flow rate of 0.45 mL/min.

The efficiency of the non-premixed combustor with flush mounted SiC igniters is on average 2.3% higher than the non-premixed combustor with Kanthal wire igniters with a maximum efficiency difference of 3.2% at the lean extinction limit and a minimum of 1.6% at $\Phi = 1.37$.

Fig. 19 shows the extinction regime for kerosene/steam/oxygen combustion; note that this combustor utilized flush mounted SiC igniters due to the heightened performance and more stable operation with methanol. Because of limitations with the experimental facility the lean extinction limit could not be determined and is represented by the approximation and structural limits shown in

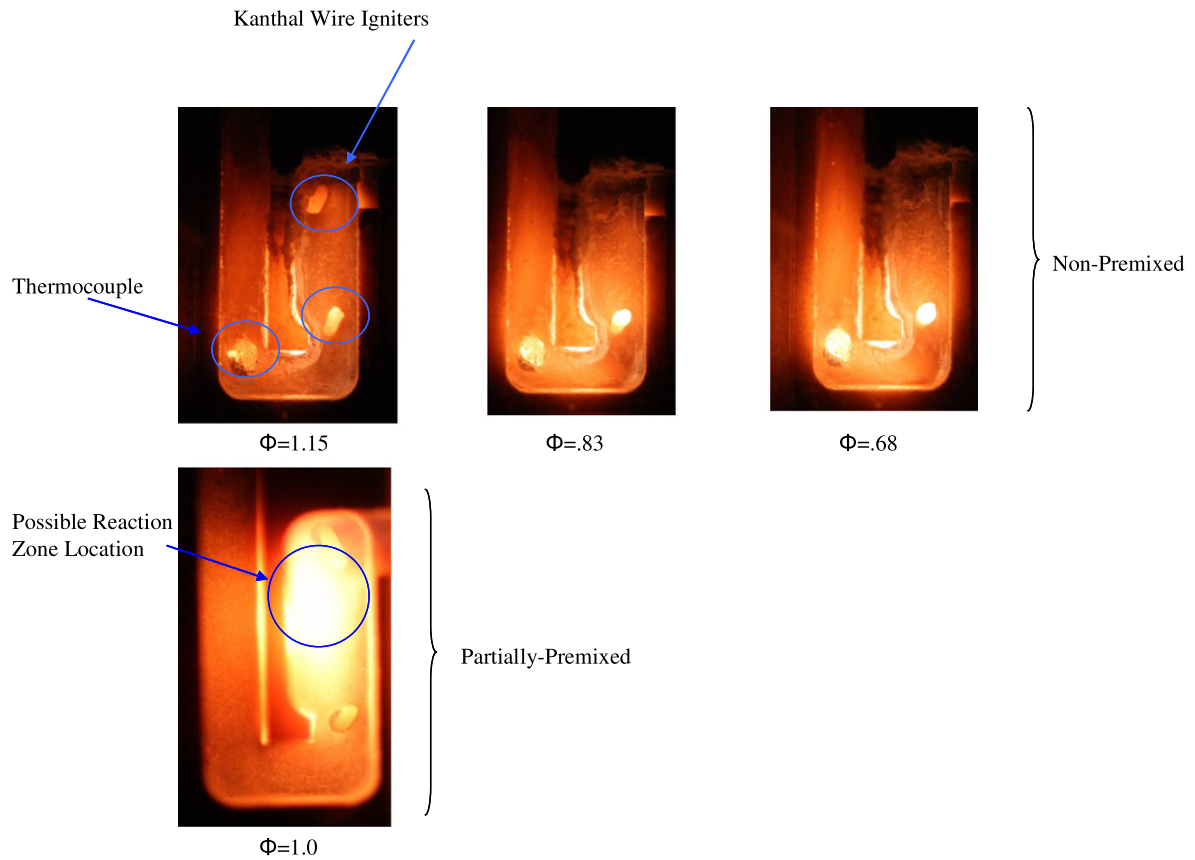


Fig. 16. Flame images of the partially-premixed and non-premixed combustor.

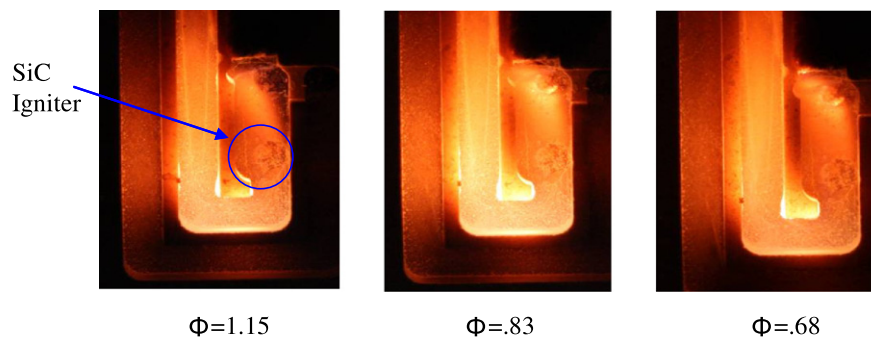


Fig. 17. Flame images with SiC igniters.

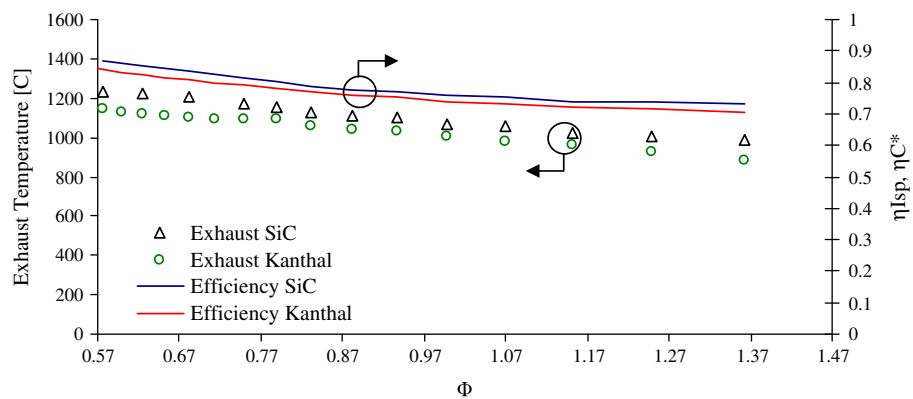


Fig. 18. Exhaust temperatures and thermal efficiencies for the non-premixed combustor with Kanthal wire igniters and SiC igniters at a methanol flow rate of 0.45 mL/min.

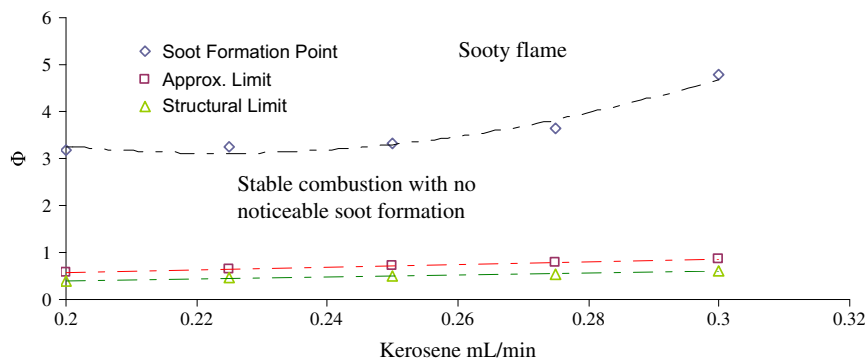


Fig. 19. Extinction regime for kerosene combustion.

Fig. 10. Because the combustor was able to support kerosene flames at very high global equivalence ratios the rich limit was defined as the point where the combustor begins producing noticeable amounts of soot. Soot formation is caused by a competition between soot production and soot oxidation and is an intrinsic property of hydrocarbon diffusion flames. The propensity for soot formation is a strong function of equivalence ratio, flame temperature, and mixing [18]. In the experimental facility the onset of soot production was identified by the deposition of soot on both the channel walls and quartz window and the yellowish white incandescence from the soot producing regions of the flame. Operation at global equivalence ratios larger than the limit for soot production would be undesirable since deposition on the channel walls would alter the characteristics of heat transfer to the reactants and may clog small passages downstream of the combustor, like a meso-scale nozzle throat, for example.

Kerosene combustion is possible over a relatively narrow range of fuel flow rates, between 0.2 mL/min and 0.3 mL/min and the global equivalence ratio limit for the formation of soot tends to increase with increase in fuel flow rate. No FREI or other instability mechanisms were observed at any condition. Fig. 20 shows the flame images and the development of the global flame structure for the kerosene flame from the soot production limit to the approximate limit for a fuel flow rate of 0.2 mL/min.

Fig. 20 shows the progression of the global flame structure from a diffusion flame with a very discrete reaction zone at very rich conditions to a condition that exhibits no visible flame at very lean conditions. At $\Phi = 2.27$ the deposition of soot on the channel walls and quartz window becomes visibly apparent, and at $\Phi = 5.31$ the soot deposition on the window is so thick that it obscures the luminosity from the channel entirely. The regions of the flame exhibiting soot nucleation and incandescence become visible at $\Phi = 1.99$.

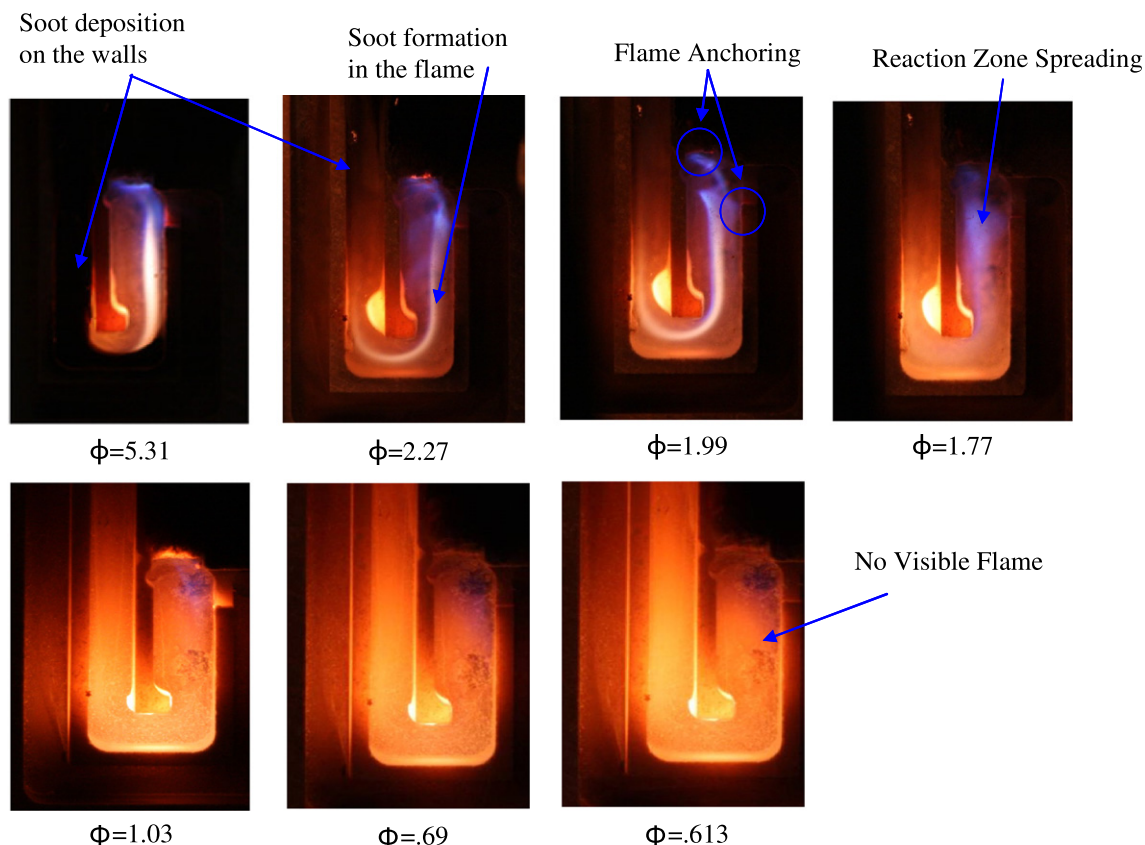


Fig. 20. Development of the kerosene global flame structure. Note that that some molten material is visible in the exhaust channel however this was produced at a condition outside the performance regime.

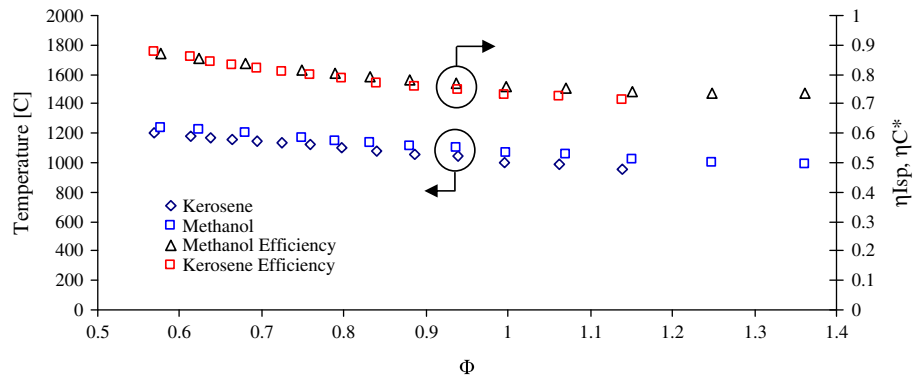


Fig. 21. Thermal performance of kerosene combustor with methanol for comparison.

In the globally fuel rich regime the flame appears to be anchored at two locations, one anchoring location is at the fuel injector and the other at downstream edge of the step inlet to the combustion chamber. This dual branching behavior is apparent at $\Phi = 2.27$ and $\Phi = 1.77$ but is most obvious at $\Phi = 1.99$. At $\Phi = 1.77$ the reaction zone spreads out, and although the anchoring locations are still apparent the surface of the flame is not as distinct. Close to the lean approximate limit the flame loses all visible emission and the combustor operates in the “flameless” mode. This combustion mode has been reported by Ahn et al. [8] in mesoscale heat recirculating combustors burning propane and air, and in macro-scale combustors with non-premixed fuel and highly pre-heated air. The reason for reaction zone broadening and “flameless” combustion in mesoscale heat-recirculating burners could be due to the small characteristic geometries and highly-preheated reactants which make it difficult to support the large temperature gradients associated with thin reaction zones [8].

Fig. 21 shows the exhaust temperatures and thermal efficiency for kerosene combustion at a fuel flow rate of 0.2 mL/min, along with methanol combustion at 0.45 mL/min. The heat inputs, calculated as the product of the Lower Heating Value (LHV) and the fuel

flow rate, are similar for the above kerosene and methanol cases at ~ 120 W and ~ 125 W respectively. In order to apply Eq. (1) to calculate the efficiency for kerosene combustion, kerosene was modeled as C_8H_{18} .

Fig. 21 shows that both the exhaust temperatures and combustor thermal efficiency for methanol and kerosene are similar, with maximum thermal efficiency of approximately 88% occurring at the lean limit. It would appear from Fig. 18 that performance of the combustor at similar heat inputs with kerosene and methanol is nearly identical, and in fact calculated estimates of the specific energy of the exhaust gas ($C_p T$) show that methanol has a higher specific energy (at the lean limit where the efficiency is highest) than kerosene and is therefore more efficient in terms of mass consumption. However, for small scale devices and micro-satellites in particular, propellant mass is not necessarily the limiting factor especially considering that small satellites tend to piggyback on larger satellites in launch fairings that are not stretched for mass (lifting capacity of the launch vehicle) but are severely constrained in volume (available space in the launch fairing) [1]. For this reason the volume specific energy ($\rho C_p T$) may be a more applicable measure of performance, this is analogous to the density-impulse or

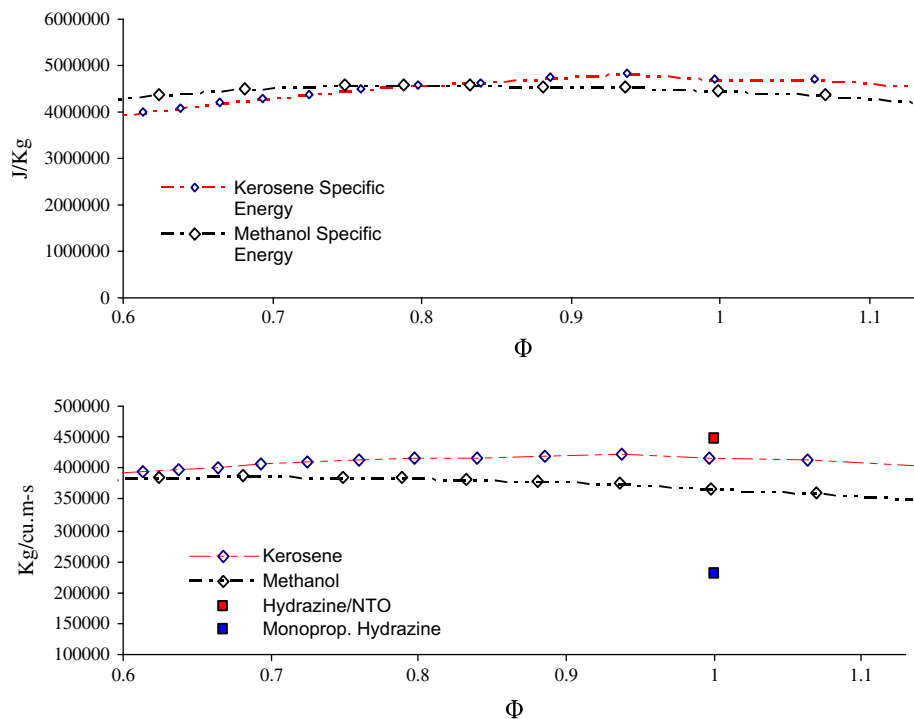


Fig. 22. Top: specific energy and bottom: density impulse for methanol (0.45 mL/min) and kerosene (0.20 mL/min).

' ρI_{sp} ' sometimes used to characterize rocket propellants and is a measure of how much volume of propellant is required to produce a certain amount of thrust. Fig. 22 shows the specific energy and density impulse from experiments for methanol, kerosene, and adiabatic values for hydrazine monopropellant and hydrazine/nitrogen tetroxide bi-propellant found in the literature. The density impulse is calculated based on the exhaust temperature and adiabatic equilibrium gas properties determined using CEA [19] assuming a 1 atm chamber pressure and expansion to vacuum. Additionally, the density impulse is calculated using the density of the fuel and oxidizer at room temperature assuming the oxidizer originates as 100% hydrogen peroxide.

The calculated density impulse of kerosene/steam/oxygen is maximum at slightly fuel lean conditions ($\Phi = 0.93$) and 5.6% smaller than the adiabatic density impulse of bi-propellant hydrazine/nitrogen tetroxide. However, heat losses from a meso-scale hydrazine thrust chamber would lower that value considerably and bring it closer to the experimental values reported above. Also, although the specific energies reported above are high, they are applied to mass flow rates in the mg/sec range with maximum output enthalpy flow rates of ~ 170 W.

4. Conclusions

A meso-scale heat recirculating combustor has been developed for use with methanol or kerosene, by utilizing steam/oxygen as an oxidizer. The steam/oxygen mixture serves as a surrogate for hydrogen peroxide. The extinction characteristics and thermal performance of both partially premixed and non-premixed configurations have been explored. In the partially-premixed configuration the extinction limits had two distinct branches, the lean branch representing flame-blow off and the rich branch representing flame-flashback. The flash-back propensity was found to be predictably sensitive to the channel geometry, where decreasing the aspect ratio at constant Re leads to stable operation at lower mass flow rates. Additionally, changing the concentration of oxygen in the inlet oxidizer stream was found to bias the extinction regime towards lower total mass flow rate due to the decrease in flame velocity in addition to changing the rich extinction criterion from flame-flashback to flame blow-off. Thermal efficiencies, defined as the efficiencies of characteristic velocity and specific impulse for this application, are largest close to the lean extinction limit for both the partially-premixed and non-premixed case with the non-premixed case having slightly higher efficiencies. It was found that changing the ignition hardware from resistance wires protruding into the combustion chamber to flush mounted SiC igniters had a positive influence on performance, stability, and combustion noise. Non-premixed combustion of kerosene demonstrated substantial soot production at high global equivalence ratios and combustion with no visible flame emission, or "flameless" combustion, close to the lean limit. Additionally, the calculated density impulse of kerosene/steam/oxygen determined using measured exhaust temperatures and simulated equilibrium combustion products are within 5.6% of the adiabatic density impulse of bi-propellant hydrazine/nitrogen tetroxide.

As discussed previously, the experimental combustor utilized a lean burning hydrogen/oxygen flame as a superheated steam/oxy-

gen source in lieu of using decomposed hydrogen peroxide. If hydrogen peroxide were used it would be expected that the extinction limits, flame dynamics, and trends in thermal performance would be the same as the experimental combustor; however, the absolute thermal performance would be slightly different. Because of the high product gas temperature of the hydrogen/oxygen flame, a hydrogen peroxide catalytic gas generator would need to operate at nearly 100% thermal efficiency to produce the same input enthalpy and hence the same thermal efficiency as the experimental combustor. Since such high efficiencies are not realistic it would be expected that the thermal performance of a combustor utilizing hydrogen peroxide would be slightly less than predicted by the experimental combustor.

Acknowledgements

This research is supported by the Missile Defense Agency (MDA). This support is gratefully acknowledged. Thanks are also due to Richard Schwarz, Alan Hickling, Jim Kiessling, and Paul Koskey for their help, support, and many useful suggestions.

References

- [1] Osiander RD, Garrison MA, Champion J. MEMS and microstructures in aerospace applications, vol. 1. New York: CRC Press, Taylor and Francis Group; 2006.
- [2] Baker A, Curiel AS, Schaffner J, Sweeting M. "You can get there from here": advanced low cost propulsion concepts for small satellites beyond LEO. *Acta Astronaut* 2005;57:288–301.
- [3] Bonafacio S. Analysis and design of a multi-phase catalytic reactor for the decomposition of hydrogen peroxide in space propulsive systems. PhD dissertation, Università degli Studi di Napoli "Federico II", Web; 2006.
- [4] Wernimont E. System trade parameter comparison of monopropellants: hydrogen peroxide vs. hydrazine and others. In: 42 AIAA/ASME/SAE/ASEE joint propulsion conference and exhibit; July 9–12, 2006.
- [5] http://femci.gsfc.nasa.gov/workshop/2003/presentations/varia/Varia-MEMS_Thruster.ppt.
- [6] Chen X, Zhou Z, Fan R. A homogeneously catalyzed micro-chemical thruster. *Sens Actuat A Phys* 2003;108:149–54.
- [7] Wu M, Wang Y, Yang V, Yetter RA. Combustion in meso-scale vortex chambers. *Proc Combust Inst* 2007;31(2):3235–42.
- [8] Ahn J, Eastwood C, Sitzki L, Ronney PD. Gas phase and catalytic combustion in heat recirculating burners. *Proc Combust Inst* 2002;29(7):957–63.
- [9] Sher I, Levinson-Sher D, Sher E. Miniaturization limitations of HCCI internal combustion engines. *Appl Therm Eng* 2009;29(2–3):400–11.
- [10] Vijayan V, Gupta AK. Combustion and heat transfer at meso scale with thermal energy recirculation. In: 47 AIAA aerospace sciences meeting; January 5–8, 2009.
- [11] Kim N, Aizumi S, Yokomari T, Kato S, Fujimori T, Maruta K. Development and scale effects of small swiss roll combustors. *Proc Combust Inst* 2007;31:3243–50.
- [12] Jones AR, Lloyd SA, Weinberg FJ. Combustion in heat exchangers. *Proc Roy Soc Lond Ser A: Math Phys Sci* 1978;60:97–115.
- [13] Vijayan V, Gupta AK. Effect of channel length on a meso-scale spiral combustor performance. In: 46th AIAA/ASME/SAE/ASEE joint propulsion conference and exhibit, Nashville, TN, Paper AIAA 2010-7065; July 25–28, 2010.
- [14] Sadasivuni V, Agrawal AK. A novel meso-scale combustion system for operation with liquid fuels. *Proc Combust Inst* 2009;32:3155–62.
- [15] Vijayan V, Gupta AK. Flame dynamics of a meso-scale heat recirculating combustor. *Appl Energy* 2010;87:3718–28.
- [16] Lewis B, Von Elbe G. Combustion flames and explosions in gases. Academic Press; 1987.
- [17] Ronney PD. Analysis of non-adiabatic heat-recirculating combustors. *Combust Flame* 2003;135:421–39.
- [18] Turns S. An introduction to combustion. 2nd ed. Boston: McGraw Hill; 2006.
- [19] <http://www.grc.nasa.gov/WWW/CEAWeb/>.